Biochemical and Biophysical Research Communications 742 (2025) 151092

Contents lists available at ScienceDirect

Biochemical and Biophysical Research Communications

journal homepage: www.elsevier.com/locate/ybbrc

Genetically encoded bioluminescent glucose indicator for biological research

Rikuto Tanaka [a], Kazunori Sugiura [b], Kenji Osabe [b], Mitsuru Hattori [b], Takeharu Nagai [a,b,c,*]

[a] Graduate School of Frontier Biosciences, The University of Osaka, Suita, Osaka, 565-0871, Japan
[b] SANKEN, The University of Osaka, Ibaraki, Osaka, 567-0047, Japan
[c] Research Institute for Electronic Science, Hokkaido University, Sapporo, Hokkaido, 001-0021, Japan

ARTICLE INFO

Keywords:
Glucose metabolism
Genetically encoded bioluminescent indicator
Bioluminescence imaging

ABSTRACT

Glucose is an essential energy source in living cells and is involved in various phenomena. To understand the roles of glucose, measuring cellular glucose levels is important. Here, we developed a bioluminescent glucose indicator called LOTUS-Glc. Unlike fluorescence, bioluminescence doesn't require excitation light when imaging. Using LOTUS-Glc, we demonstrated drug effect evaluation, concurrent use with the optogenetic tool in HEK293T cells, and the measurement of light-dependent glucose fluctuations in plant-derived protoplasts. LOTUS-Glc would be a useful tool for understanding the roles of glucose in living organisms.

1. Introduction

Glucose is one of the most common energy sources in living organisms and is essential for cell growth, cell division, and homeostasis [1]. Intracellular glucose is broken down into pyruvate by glycolysis in the cytoplasm. The pyruvate is then transported to the mitochondria, where it is converted into acetyl-CoA and undergoes further processes, including the citric acid cycle, oxidative phosphorylation, and the electron transport chain. Metabolites produced during these processes are used for lipid and nucleic acid synthesis, and also function as ROS scavengers and signaling molecules [2,3].

Since intracellular glucose concentration is an important parameter for understanding the various roles of glucose, multiple methods have been developed to measure it. Glucose labeling with isotopes or chemical dyes can detect the increase in glucose levels [4,5]. On the other hand, indicators using fluorescent proteins can also detect the decrease in glucose levels. To that end, several fluorescent glucose indicators have been developed that can observe fluctuations in cellular glucose levels [6–8].

Although fluorescent indicators are powerful tools for observing cellular phenomena, they require excitation light for observation, which can cause the phototoxicity and autofluorescence of endogenous proteins or molecules. Additionally, the use of excitation light can complicate fluorescence measurements in situations involving optogenetic tools and light-dependent phenomena. Bioluminescent indicators solve these problems. A bioluminescent protein, luciferase, catalyzes the oxidation of its substrate, luciferin, resulting in light emission. Therefore, a signal can be obtained without excitation light, avoiding related issues with excitation light. Leveraging these advantages, several bioluminescent indicators have been used to observe the control of membrane voltage using an optogenetic tool [9,10], to observe light-dependent pH change in cyanobacteria [11], and to conduct high-throughput drug screenings [12].

Given this background, we attempted to develop a bioluminescent glucose indicator capable of detecting fluctuations through bioluminescence color changes. In this research, we demonstrated the utility of our indicator by evaluating the effect of drug treatment and an optogenetics tool, and by detecting glucose fluctuations in plant-derived protoplasts.

2. Material and methods

2.1. Gene constructs

The DNA sequences of MglB, ECFP, Citrine, and miniSOG2 were obtained from the plasmid of pcDNA3.1_FLII12Pglu-700μΔ6 [8] (Addgene plasmid #17866) and pcDNA3.1_miniSOG2 T2A H2B-EGFP [13] (Addgene plasmid #87410), respectively. The sequence of nanoKAZ was synthesized artificially. Each DNA fragment was amplified by PCR using KOD-Plus (Toyobo Life Science) with specific primer pairs. A

* Corresponding author. SANKEN, The University of Osaka, Ibaraki, Osaka, 567-0047, Japan.
E-mail address: ng1@sanken.osaka-u.ac.jp (T. Nagai).

https://doi.org/10.1016/j.bbrc.2024.151092
Received 5 November 2024; Accepted 27 November 2024
Available online 28 November 2024

mutation in MglB (D236A) was also inserted using specific primers. Each amplified fragment was connected by over-lap PCR and subcloned into a linearized plasmid by hot-fusion method [14]. The vectors selected were $pRSET_B$ for bacterial expression, pcDNA3 for mammalian expression, and pRI201_AN for plant expression. A chloroplast localization signal, the ribulose bisphosphate carboxylase small chain 1A (RBCS1a) [15] sequence was fused at the N-terminal of LOTUS-Glc and LOTUS-Glc (D236A) with a Gly-Gly-Ser-Gly-Gly linker. For the co-expression of miniSOG2 and LOTUS-Glc, we connected the LOTUS-Glc and miniSOG2 with self-cleavable P2A peptide [16]. Transformation of *Escherichia coli* (*E. coli*) strain XL10-Gold was performed using the heat shock method, and a single colony was cultured in 2 mL of LB media with 0.1 mg/ml ampicillin at 37 °C overnight. Small-scale DNA preparation was performed by alkaline-SDS lysis from collected bacterial pellets. The plasmid sequences were confirmed by dye terminator cycle sequencing using the BigDye Terminator v1.1 cycle sequencing kit (Thermo Fisher Scientific). The DNA sequences of LOTUS-Glc and its variants are shown in Note S1.

2.2. Protein purification

The recombinant protein was expressed in *E. coli* strain JM109(DE3) by culturing in 200 mL LB media containing 0.1 mg/ml carbenicillin at 23 °C for 60 h. Cultured cells were collected and disrupted with a French press (Glen Mills). The recombinant protein was purified from the supernatant of the cell lysate using Ni-NTA agarose affinity columns (QIAGEN) and followed by a buffer exchange (20 mM HEPES, pH7.4) with a desalting column PD-10 (GE Healthcare). The purified protein concentration was determined by the Bradford method (Protein Assay kit, Bio-Rad).

2.3. In vitro characterization

For luminescence spectrum measurements, 100 μL of 100 nM protein solution and 100 μL of 5 μM luciferin, coelenterazine-h (Wako) solution were mixed. The luminescence spectrum was measured using a multi-channel spectrometer, PMA-12 (Hamamatsu photonics), after adding coelenterazine-h to the purified protein in 20 mM HEPES buffer (pH 7.4). The fluorescence spectrum was measured using a spectrofluorometer, F-7000 (HITACHI) by 435 ± 5 nm excitation. The ratio (530/480 nm) was calculated from the peak intensities of the emission wavelengths. The dynamic range was calculated by dividing the ratio value in the presence of glucose (Wako) by the ratio value in the absence of glucose. Using data analysis software (LightStone, Origin7), titration curves were obtained by fitting the Hill model.

2.4. Mammalian cell experiments

HEK293T cells (RIKEN BRC Cell Bank RCB2202) were cultured in Dulbeccos's modified Eagle's medium (DMEM) containing 10 % fetal bovine serum at 37 °C. One day before transfection, cells were trypsinized and transferred to a 35 mm glass-bottom dish. Cells were transfected with expression plasmid by using polyethylene imine (Polyscience, PEI Max) according to the manufacturer's instructions. Before imaging, the cell culture medium was exchanged with Dulbeccos's phosphate buffered saline (D-PBS) or DMEM/F12 containing 10 % Hank's balanced salt solution (HBSS), adding 200 μL of each solution and incubated for 1 h. 700 μL of luciferin, furimazine (Promega, Nano-Glo®Luciferase Assay System) was added to the cells. 100 μL of 250 mM Glucose solution or 100 μL of 100 μM Phloretin (Tokyo Chemical Industry) solution were added to the cells along with furimazine. The exposure time was 1 min for D-PBS and 2 min for DMEM/F12 containing 10 % HBSS in case of luminescence and 300 ms for fluorescence. Cell images were acquired using an inverted microscopy (Olympus, IX83) equipped with a 40 × objective lens (Olympus, UPLFLN40x), an EMCCD camera (Andor, iXon Ultra), light source (Olympus, U-HGLGPS), and emission filters (Olympus, U-FCFP as C-channel, U-FYFP as Y-channel). The laser power for fluorescence imaging was 6 %. To excite miniSOG2 for ROS production, irradiation through U-FCFP was used at an intensity of 50 % laser power and an exposure time of 90 s. Cells were incubated with Phloretin overnight, and cell suspensions were prepared by trypsinization. The spectra of cell suspensions were measured using a plate reader (CORONA). The emission peak ratio of the indicator in the captured image was calculated using ImageJ. The pseudo-color image was arranged using Metamorph (Molecular Devices). The ROS Assay Kit -Highly Sensitive DCFH-DA (DOJINDO) was used to measure ROS production following the provided protocol. The fluorescence intensity of cell suspensions at 526 nm was measured using F-7000 (HITACHI) before and after light irradiation.

2.5. Preparation and bioluminescence measurement of protoplasts

Nicotiana benthamiana leaves were transfected with plant expression plasmids via GV3101 *Agrobacterium tumefaciens* following an established method [17]. Transfected leaves were collected and cut into pieces. The cut leaves were soaked in the enzyme solution (1 % cellulase, 0.6 % macerozyme, 400 mM mannitol, 20 mM KCl, 10 mM $CaCl_2 \cdot 2H_2O$, 20 mM MES, pH5.7) and incubated in the dark for 5–7 h until the leaves were digested. After digestion, protoplasts were collected and washed with wash buffer (400 mM mannitol, 20 mM KCl, 10 mM $CaCl_2 \cdot 2H_2O$, 10 mM MES, pH5.7). Protoplasts were kept on ice during washing. Finally, protoplasts were suspended with suspension buffer (400 mM mannitol, 15 mM $MgCl_2$, 10 mM HEPES, pH 7.4) with and without bicarbonate (5 mM $NaHCO_3$) and incubated under dark conditions (covered with aluminum foil) and light conditions (60 μmol/m^2/sec) overnight. Furimazine was added to protoplasts just before the luminescence spectrum was measured using a plate reader.

2.6. Confirmation of the localization of LOTUS-Glc in protoplast

Localization of LOTUS-Glc in protoplast was observed using inverted microscopy (Nikon, Ti-2) equipped with a confocal unit (Andor, Dragon fly200), a 100 × objective lens (Nikon, CFI Plan ApochromatλD 100x Oil), an EMCCD camera (Andor, iXon Ultra), fluorescence filters (521/38 nm for Citrine, 700/75 nm for autofluorescence), a 488 nm laser for Citrine, and a 637 nm laser for autofluorescence.

3. Results

3.1. In vitro characterization

There are two designs of ratiometric bioluminescent indicator: one composed of YFP and luciferase, and another composed of YFP, CFP, and luciferase [9,10]. The mechanism of both designs alters Bioluminescence Resonance Energy Transfer (BRET) efficiency through conformational changes. Because the former design showed no response to glucose (Fig. S1), the latter design was chosen. The indicator comprises four types of proteins: MglB, a glucose-binding protein [18], Citrine [19], ECFP [20], and nanoKAZ [21], in accordance with previously reported indicator designs [8,10] (Fig. 1A). Screening was based on the dynamic range, calculated from the emission peak ratio (530/480 nm) variations at glucose concentrations ranging from 0 mM to 100 mM. After the screening, the construction that showed the highest dynamic range was named LOTUS-Glc (Luminescent Optical Tool for Universal Sensing of Glucose). The previous fluorescent glucose indicator, FLII12Pglu-700μΔ6, had a dynamic range of 36 % (Fig. S2), while LOTUS-Glc has a much higher dynamic range of 200 % (Fig. 1B). It has been reported that the mutation in MglB (D236A) abolishes glucose binding [22], we introduced this mutation and named the variant LOTUS-Glc (D236A) (Fig. 1C). Because MglB was originally reported as a glucose and galactose-binding protein [18], its specificity must be evaluated. We confirmed the specificity of the indicator for other

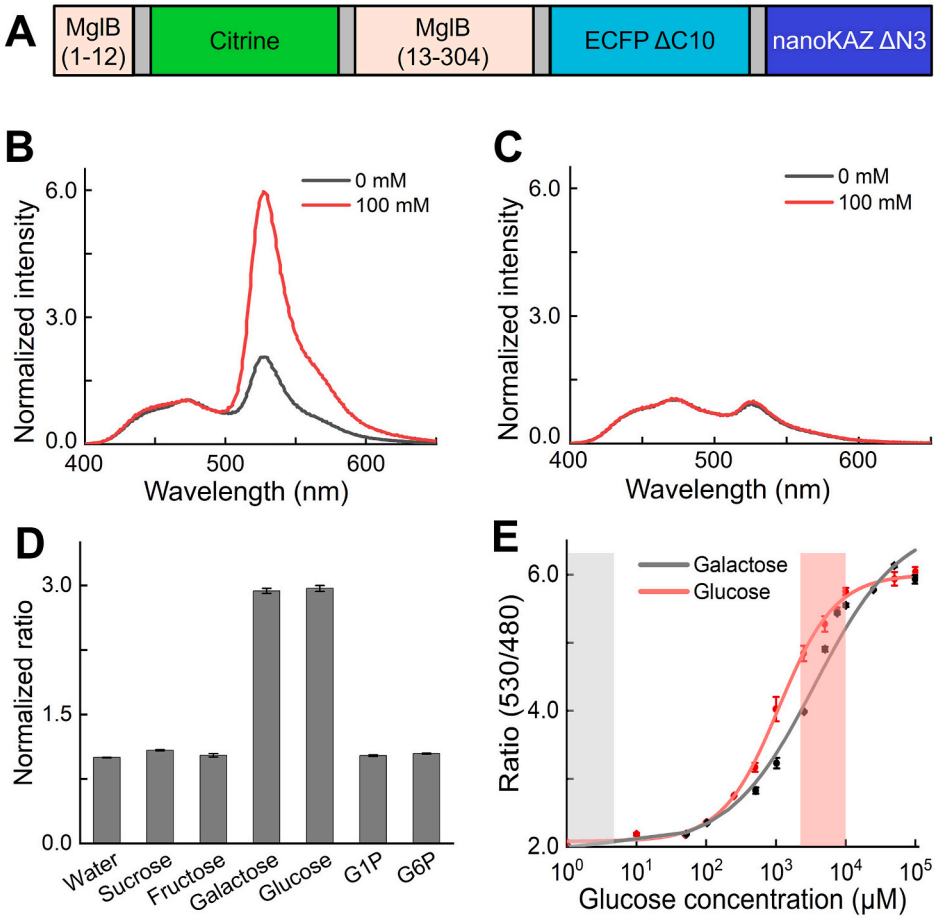

Fig. 1. In vitro characterization of LOTUS-Glc. (A) Schematic diagram of LOTUS-Glc. The numbers in MglB mean the amino acid sequence used. (B and C) Luminescence spectrum of LOTUS-Glc (B) and LOTUS-Glc (D236A) (C). Normalization was performed using the intensity at 480 nm. (D) Binding selectivity of LOTUS-Glc. The final concentration of each compound was 100 mM. Normalization was performed using the ratio of water. (E) Dose-response curve of LOTUS-Glc to different galactose and glucose concentrations. Gray and red zones showed the general galactose (Gray) and glucose (Red) concentrations in plasma. These data were taken by a multichannel spectrometer. The data represents the means ± standard deviation (n = 3). (For interpretation of the references to color in this figure legend, the reader is referred to the Web version of this article.)

compounds, such as galactose, sucrose, fructose, Glucose-1-phosphate (G1P), and Glucose-6-phosphate (G6P). As predicted, LOTUS-Glc also responded to galactose but no other compounds (Fig. 1D). To evaluate the affinity of LOTUS-Glc to glucose, we measured the emission peak ratio (530/480 nm) in response to glucose concentration (Fig. 1E). According to previous reports [6–8], K_d values suitable for observing cellular glucose concentrations range from several hundred μM to several mM. From the dose-response curve, the K_d value of LOTUS-Glc was 1.1 mM. Therefore, it is suitable for live-cell imaging in general physiological conditions. Generally, physiological galactose concentrations are much lower than glucose [23,24]. Since the K_d value of LOTUS-Glc for galactose was 3.5 mM, we can disregard the effect of galactose during observation.

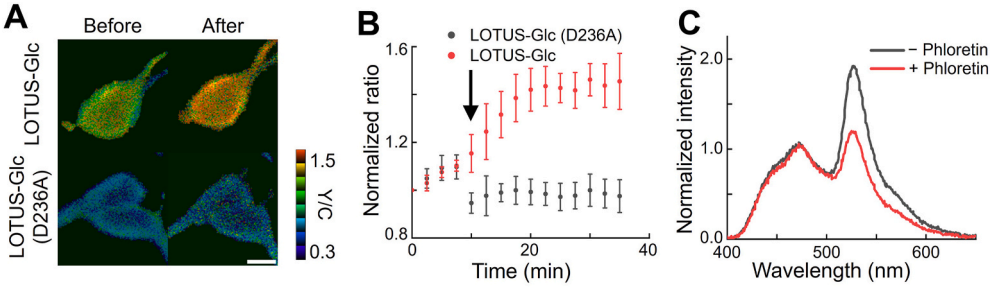

Fig. 2. Application of LOTUS-Glc to HEK293T cells. (A) Pseudo-color images of cells expressing LOTUS-Glc before and after the addition of glucose. The scale bar represents 10 μm. (B) The time-course of the ratio changes of cells before and after the addition of glucose. The black arrow in the graph means the time point of glucose addition. Normalization was performed using the ratio at 0 min. The data represent the means ± standard deviation (LOTUS-Glc: 18 cells, LOTUS-Glc (D236A): 15 cells). (C) Luminescence spectrum of cell suspension expressing LOTUS-Glc with and without the addition of Phloretin. Spectrum was taken by a plate reader. Normalization was performed using the intensity at 480 nm. (For interpretation of the references to color in this figure legend, the reader is referred to the Web version of this article.)

3.2. Glucose imaging and evaluation of drug treatment in mammalian cells

To verify LOTUS-Glc ability to detect changes in glucose levels in mammalian cells, the indicator was introduced into HEK293T cells. Generally, glucose in mammalian cells is dependent on external supply. Therefore, it is possible to control intracellular glucose by changing its level in the culture media [6,7]. For cells cultured in glucose-free media, we observed changes in bioluminescence upon adding glucose. After adding glucose, the luminescence intensity ratio in the yellow and cyan channels (Y/C) increased significantly only in LOTUS-Glc (Fig. 2A and B). Next, we evaluated the effect of luminescence intensity decay on the ratio. Although a slight increase in the ratio was observed for both LOTUS-Glc and LOTUS-Glc (D236A), this increase was small compared to the ratio change due to the addition of glucose, suggesting that the fluctuation in the ratio due to the attenuation of luminescence intensity can be ignored. (Fig. S3).

Since the bioluminescent indicators are often applied for drug screening, we assessed the impact of Phloretin, a glucose transporter (GLUT) inhibitor, on cells. Intracellular glucose levels can be controlled by inhibiting GLUT, which uptakes glucose. After the cells were incubated with Phloretin overnight, we measured the luminescence spectra of the cell suspensions. As a result, the Phloretin treatment decreased the ratio (530/480 nm) compared to the non-treatment (Fig. 2C). Conversely, no difference was observed in LOTUS-Glc (D236A) with or without Phloretin (Fig. S4), confirming LOTUS-Glc's ability to detect glucose decrease caused by Phloretin. We also confirmed a time-dependent decrease in the ratio after the addition of Phloretin (Fig. S5). These results suggest that LOTUS-Glc in HEK293T cells can measure both increases and decreases in glucose. The K_d value of LOTUS-Glc is suitable for observing glucose kinetics, making it an effective tool for evaluating drug treatments.

3.3. Evaluation of glucose fluctuations in plant cells

Plants change their metabolism in response to the environment. Especially, light is one of the most important factors. When measuring fluorescence, it is necessary to irradiate the plant with excitation light (several hundreds to thousands μmol/m^2/sec), which is much higher than the light compensation point in *Nicotiana tabacum* (20–35 μmol/m^2/sec) [25]. In contrast, the luminescence intensity of Nluc, which has the same amino acid as nanoKAZ, is much lower than the light compensation points when expressed at micromolar concentrations in cells (around several hundred nmol/m^2/sec) [26–28]. Therefore, bioluminescence, which doesn't require excitation light, is suitable for evaluating the effect of light on plants. Under light conditions, glucose is synthesized via photosynthesis and stored as a starch in chloroplasts. Stored starch is decomposed under dark conditions [29]. These factors suggest that controlling photosynthesis and light/dark conditions results in different glucose fluctuations. Protoplasts are cells whose cell walls have been removed by enzyme treatment. In plant-derived protoplasts, bicarbonate is used as a carbon source instead of carbon dioxide. Therefore, it is possible to control glucose production through photosynthesis or starch decomposition by using the presence or absence of bicarbonate and light/dark conditions [30,31]. In this study, we localized LOTUS-Glc to the cytoplasm and chloroplasts and observed glucose fluctuations within the protoplasts. Protoplasts were prepared from tobacco leaf cells transfected with our indicators, and we confirmed their localization (Fig. 3A). Protoplasts were left overnight in the presence or absence of bicarbonate under light or dark conditions. We then compared the ratio (530/480 nm) changes between light and dark conditions. As a result, in the chloroplasts, the change was 1 % in the presence of bicarbonate (Figs. 3B), and 15 % in the absence of bicarbonate (Fig. 3D). The decrease in the ratio difference in the presence of bicarbonate is likely because bicarbonate serves as a carbon source under light conditions, leading to glucose production by photosynthesis.

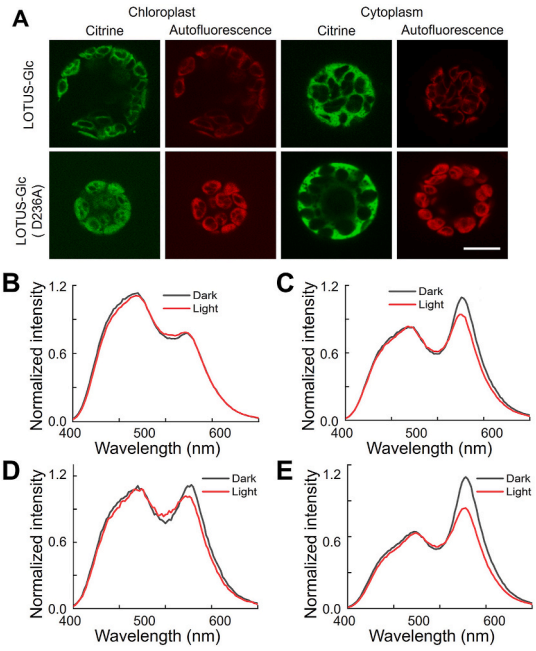

Fig. 3. Application to protoplasts. (A) Localization of LOTUS-Glc in protoplasts. The scale bar represents 10 μm. The contrast in each image was automatically modified. (B–E) Luminescence spectrum of protoplast expressing LOTUS-Glc. (B) presence of bicarbonate, chloroplast. (C) presence of bicarbonate, cytoplasm. (D) absence of bicarbonate, chloroplast. (E) absence of bicarbonate, cytoplasm. Normalization was performed at 480 nm intensity.

On the other hand, in the cytoplasm, the change was 21 % in the presence of bicarbonate (Figs. 3C) and 27 % in the absence of bicarbonate (Fig. 3E), suggesting that the effect of glucose production in the chloroplasts via photosynthesis is limited in the cytoplasm. In the case of LOTUS-Glc (D236A), no changes in the signal were observed (Fig. S6). These results indicated that LOTUS-Glc can effectively measure glucose fluctuations in plant cells.

3.4. A combination of optogenetic tool and LOTUS-Glc

Since bioluminescence imaging does not require excitation light, it offers convenience when combined with optogenetic tools. Several bioluminescent indicators have been used with optogenetic tools [9,32]. In this research, we also attempted to detect glucose level variations with an optogenetic tool utilizing LOTUS-Glc. GLUT activates glucose uptake in the presence of reactive oxygen species (ROS) [2]. The fluorescent protein, miniSOG2, generates ROS while also producing fluorescence upon excitation [13], thereby allowing manipulation of GLUT activity. HEK293T cells expressing miniSOG2 and LOTUS-Glc were irradiated with blue light to evaluate glucose fluctuation (Fig. 4A). As a result, the normalized Y/C ratio in LOTUS-Glc increased after blue light irradiation in cells expressing miniSOG2 (Fig. 4B). This increase did not occur with LOTUS-Glc (D236A) (Fig. S7). We also confirmed ROS production upon light irradiation in HEK293T cells expressing miniSOG2 (Fig. S8). These results suggest that LOTUS-Glc is capable of evaluating the effect of miniSOG2 activation on glucose levels in cells over time.

4. Discussion

In this research, we developed a bioluminescent glucose indicator, LOTUS-Glc, based on the previous indicators [8,10]. LOTUS-Glc is enabled to detect the intracellular glucose concentration fluctuations through BRET involving luciferase and two fluorescent proteins. This detection method was shown to be compatible with optogenetic tools, and useful for analyzing glucose fluctuations in plant cells and

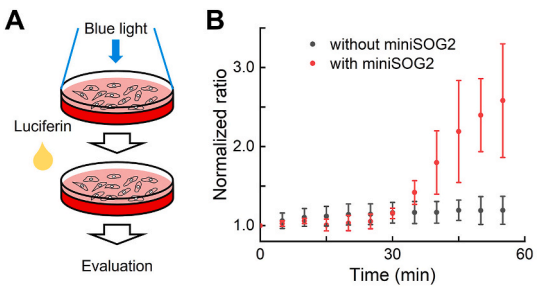

Fig. 4. Evaluation of optogenetics tool effect with LOTUS-Glc in HEK293T cells. (A) Schematic illustration of experimental flow. Luciferin was added after the blue light irradiation. (B) The time course of the ratio changes after blue light irradiation. Normalization was performed using the ratio at 0 min. The data represents the means ± standard deviation (15 cells). (For interpretation of the references to color in this figure legend, the reader is referred to the Web version of this article.)

evaluating drug treatments.

In LOTUS-Glc, the dynamic range of the bioluminescence response to glucose was higher than that of the previous fluorescent indicator (Fig. 1A–S2) [8]. Although comparing fluorescence with bioluminescence is challenging, introducing luciferase to enhance the BRET factor likely contributes to this result. In the FLII12Pglu-700μΔ, Förster Resonance Energy Transfer (FRET) occurs only between ECFP and Citrine [8], whereas LOTUS-Glc allows BRET among three entities: nanoKAZ to ECFP, nanoKAZ to Citrine, and ECFP to Citrine. This suggests that the bioluminescence ratiometric indicator functions more effectively with appropriately adjusted positional relationships, such as through the use of linkers.

We must consider photobleaching or phototoxicity when using fluorescent protein [33–35]. While fluorescence imaging requires excitation light for observation, bioluminescence imaging does not use any excitation light, thereby avoiding problems associated with excitation light. A comparison of the ratio stability between LOTUS-Glc and FLII12Pglu-700μΔ6 revealed a slight change in the ratio for LOTUS-Glc, while a clear increase in the ratio was observed for FLII12Pglu-700μΔ6 (Figs. S3 and S9). This increase in the ratio for FLII12Pglu-700μΔ6 may have resulted from phototoxicity or photobleaching due to excitation light irradiation. Because bioluminescence intensity varies depending on the environmental factors and the amount of luciferin and luciferase, we must be careful when analyzing the bioluminescence values. However, LOTUS-Glc enables ratiometric measurement, it is possible to eliminate various influences and enable more reliable quantitative analysis.

Because of the low background signal and high sensitivity, bioluminescent indicators are often applied for high-throughput analyses such as drug screening [12]. In this research, we confirmed that LOTUS-Glc can evaluate the effect of Phloretin on cell suspensions. Therefore, these assays are applicable for high-throughput drug screening that focuses on regulating glucose levels, such as antidiabetic drugs. In addition, high-throughput screening has been performed using plant-derived protoplasts in the search for molecules that alter plant function [36]. Therefore, LOTUS-Glc can be applied for molecule screenings affecting glucose levels in both mammalian and plant cells.

ROS generation from miniSOG2 altered glucose levels in cells as demonstrated by LOTUS-Glc. It is thought that this ROS affected the cellular glucose transporter GLUT1, altering expression levels, translocating to the plasma membrane, and activating glucose uptake [2]. During the activation process of GLUT1, ROS-activated AMPK released Stomatin or TXNIR from GLUT1, resulting in the activation of glucose uptake [37,38]. Activation of glucose uptake through GLUT1 occurs within a relatively short time (within 1 h) [2]. Since the ratio of LOTUS-Glc increased over a short period, we can speculate that this increase reflects the activation of glucose uptake through GLUT1.

In the protoplast results, the ratio under dark conditions was higher than under light conditions except for the presence of bicarbonate in the chloroplast. In plants, glucose synthesized through photosynthesis is stored as a starch, and its decomposition is upregulated under dark conditions [29]. Therefore, this higher glucose concentration under dark conditions can be attributed to the decomposition of starch.

In addition to the applications demonstrated in this study, bioluminescence imaging has also been used for tasks challenging for fluorescence imaging, such as deep tissue imaging or imaging of freely moving mice [39,40]. We believe that bioluminescent indicators will become important tools as such applications are expected to expand in the future.

CRediT authorship contribution statement

Rikuto Tanaka: Data curation, Formal analysis, Funding acquisition, Investigation, Validation, Writing – original draft. **Kazunori Sugiura:** Validation. **Kenji Osabe:** Validation. **Mitsuru Hattori:** Funding acquisition, Investigation, Validation, Writing – original draft. **Takeharu Nagai:** Funding acquisition, Project administration, Supervision, Validation, Writing – review & editing.

Data availability statements

All data generated or analyzed during this study are included in this published article and its supplementary data.

Funding sources

This study was partially supported by grants from the Ministry of Education, Culture, Sports, Science, and Technology (MEXT) (No. 18H05410 to T.N.), the Japan Society for the Promotion of Science (JSPS) (No. 22K05143 to M.H.), the JST CREST Program (No. JPMJCR20H9 to T.N.), the Japan Science and Technology Agency (JST) SPRING (No. JPMJSP2138 to R.T.), the Takeda Science Foundation (to T.N.), and the Uehara Memorial Foundation (to T.N.).

Declaration of competing interest

We declare that we have no known competing financial interests or personal relationships that could have appeared to influence the work reported in this paper.

Appendix A. Supplementary data

Supplementary data to this article can be found online at https://doi.org/10.1016/j.bbrc.2024.151092.

References

[1] R.J. DeBerardinis, J.J. Lum, G. Hatzivassiliou, C.B. Thompson, The biology of cancer: metabolic reprogramming fuels cell growth and proliferation, Cell Metabol. 7 (2008) 11–20, https://doi.org/10.1016/j.cmet.2007.10.002.
[2] D.C. Liemburg-Apers, P.H.G.M. Willems, W.J.H. Koopman, S. Grefte, Interactions between mitochondrial reactive oxygen species and cellular glucose metabolism, Arch. Toxicol. 89 (2015) 1209–1226, https://doi.org/10.1007/s00204-015-1520-y.
[3] J. Sheen, Master regulators in plant glucose signaling networks, J. Plant Biol. 57 (2014) 67–79, https://doi.org/10.1007/s12374-014-0902-7.
[4] P. Trinder, Determination of glucose in blood using glucose oxidase with an alternative oxygen acceptor, Ann. Clin. Biochem. 6 (1969) 24–27, https://doi.org/10.1177/000456326900600108.
[5] A. Fatangare, A. Svatoš, Applications of 2-deoxy-2-fluoro-d-glucose (FDG) in plant imaging: past, present, and future, Front. Plant Sci. 7 (2016) 1–11, https://doi.org/10.3389/fpls.2016.00483.
[6] M. Mita, M. Ito, K. Harada, I. Sugawara, H. Ueda, T. Tsuboi, T. Kitaguchi, Green fluorescent protein-based glucose indicators report glucose dynamics in living cells, Anal. Chem. 91 (2019) 4821–4830, https://doi.org/10.1021/acs.analchem.9b00447.
[7] M. Mita, I. Sugawara, K. Harada, M. Ito, M. Takizawa, K. Ishida, H. Ueda, T. Kitaguchi, T. Tsuboi, Development of red genetically encoded biosensor for

visualization of intracellular glucose dynamics, Cell Chem. Biol. 28 (2022) 1–11, https://doi.org/10.1016/j.chembiol.2021.06.002.
[8] H. Takanaga, B. Chaudhuri, W.B. Frommer, GLUT1 and GLUT9 as major contributors to glucose influx in HepG2 cells identified by a high sensitivity intramolecular FRET glucose sensor, Biochim. Biophys. Acta Biomembr. 1778 (2008) 1091–1099, https://doi.org/10.1016/j.bbamem.2007.11.015.
[9] S. Inagaki, H. Tsutsui, K. Suzuki, M. Agetsuma, Y. Arai, Y. Jinno, G. Bai, M. J. Daniels, Y. Okamura, T. Matsuda, T. Nagai, Genetically encoded bioluminescent voltage indicator for multi-purpose use in wide range of bioimaging, Sci. Rep. 7 (2017) 42398, https://doi.org/10.1038/srep42398.
[10] N. Komatsu, K. Terai, A. Imanishi, Y. Kamioka, K. Sumiyama, T. Jin, Y. Okada, T. Nagai, M. Matsuda, A platform of BRET-FRET hybrid biosensors for optogenetics, chemical screening, and in vivo imaging, Sci. Rep. 8 (2018) 1–14, https://doi.org/10.1038/s41598-018-27174-x.
[11] S. Nakamura, N. Fu, K. Kondo, K.I. Wakabayashi, T. Hisabori, K. Sugiura, A luminescent Nanoluc-GFP fusion protein enables readout of cellular pH in photosynthetic organisms, J. Biol. Chem. 296 (2021) 1–11, https://doi.org/10.1074/jbc.RA120.016847.
[12] B. Baljinnyam, M. Ronzetti, A. Simeonov, Advances in luminescence-based technologies for drug discovery, Expet Opin. Drug Discov. 18 (2023) 25–35, https://doi.org/10.1080/17460441.2023.2160441.
[13] K. Makhijani, T.L. To, R. Ruiz-González, C. Lafaye, A. Royant, X. Shu, Precision optogenetic tool for selective single- and multiple-cell ablation in a live animal model System, Cell Chem. Biol. 24 (2017) 110–119, https://doi.org/10.1016/j.chembiol.2016.12.010.
[14] C. Fu, W.P. Donovan, O. Shikapwashya-Hasser, X. Ye, R.H. Cole, Hot fusion: an efficient method to clone multiple DNA fragments as well as inverted repeats without ligase, PLoS One 9 (2014) 1–20, https://doi.org/10.1371/journal.pone.0115318.
[15] A. Theologis, J.R. Ecker, C.J. Palm, N.A. Federspiel, S. Kaul, O. White, J. Alonso, H. Altafi, R. Araujo, C.L. Bowman, S.Y. Brooks, E. Buehler, A. Chan, Q. Chao, H. Chen, R.F. Cheuk, C.W. Chin, M.K. Chung, L. Conn, A.B. Conway, A.R. Conway, T.H. Creasy, K. Dewar, P. Dunn, P. Etgu, T.V. Feldblyum, J.D. Feng, B. Fong, C. Y. Fujii, J.E. Gill, A.D. Goldsmith, B. Haas, N.F. Hansen, B. Hughes, L. Huizar, J. L. Hunter, J. Jenkins, C. Johnson-Hopson, S. Khan, E. Khaykin, C.J. Kim, H.L. Koo, I. Kremenetskaia, D.B. Kurtz, A. Kwan, B. Lam, S. Langin-Hooper, A. Lee, J.M. Lee, C.A. Lenz, J.H. Li, Y.P. Li, X. Lin, S.X. Liu, Z.A. Liu, J.S. Luros, R. Maiti, A. Marziali, J. Militscher, M. Miranda, M. Nguyen, W.C. Nierman, B.I. Osborne, G. Pai, J. Peterson, P.K. Pham, M. Rizzo, T. Rooney, D. Rowley, H. Sakano, S.L. Salzberg, J. R. Schwartz, P. Shinn, A.M. Southwick, H. Sun, L.J. Tallon, G. Tambunga, M. J. Toriumi, C.D. Town, T. Utterback, S. Van Aken, M. Vaysberg, V.S. Vysotskaia, M. Walker, D. Wu, G. Yu, C.M. Fraser, J.C. Venter, R.W. Davis, Sequence and analysis of chromosome 1 of the plant Arabidopsis thaliana, Nature 408 (2000) 816–820, https://doi.org/10.1038/35048500.
[16] J.H. Kim, S.R. Lee, L.H. Li, H.J. Park, J.H. Park, K.Y. Lee, M.K. Kim, B.A. Shin, S. Y. Choi, High cleavage efficiency of a 2A peptide derived from porcine teschovirus-1 in human cell lines, zebrafish and mice, PLoS One 6 (2011) 1–8, https://doi.org/10.1371/journal.pone.0018556.
[17] I.A. Sparkes, J. Runions, A. Kearns, C. Hawes, Rapid, transient expression of fluorescent fusion proteins in tobacco plants and generation of stably transformed plants, Nat. Protoc. 1 (2006) 2019–2025, https://doi.org/10.1038/nprot.2006.286.
[18] N.K. Vyas, M.N. Vyas, F.A. Quiocho, Sugar and signal-transducer binding sites of the Escherichia coli galactose chemoreceptor protein, Science 242 (1988) 1290–1295, https://doi.org/10.1126/science.3057628.
[19] O. Griesbeck, G.S. Baird, R.E. Campbell, D.A. Zacharias, R.Y. Tsien, Reducing the environmental sensitivity of yellow fluorescent protein. Mechanism and applications, J. Biol. Chem. 276 (2001) 29188–29194, https://doi.org/10.1074/jbc.M102815200.
[20] R. Heim, R.Y. Tsien, Engineering green fluorescent protein for improved brightness, longer wavelengths and fluorescence resonance energy transfer, Curr. Biol. 6 (1996) 178–182, https://doi.org/10.1016/S0960-9822(02)00450-5.
[21] S. Inouye, J. Sato, Y. Sahara-Miura, S. Yoshida, H. Kurakata, T. Hosoya, C6-Deoxy coelenterazine analogues as an efficient substrate for glow luminescence reaction of nanoKAZ: the mutated catalytic 19kDa component of Oplophorus luciferase, Biochem. Biophys. Res. Commun. 437 (2013) 23–28, https://doi.org/10.1016/j.bbrc.2013.06.026.
[22] M. Fehr, S. Lalonde, I. Lager, M.W. Wolff, W.B. Frommer, In vivo imaging of the dynamics of glucose uptake in the cytosol of COS-7 cells by fluorescent nanosensors, J. Biol. Chem. 278 (2003) 19127–19133, https://doi.org/10.1074/jbc.M301333200.
[23] P. Schadewaldt, H.W. Hammen, K. Loganathan, A. Bodner-Leidecker, U. Wendel, Analysis of concentration and 13C enrichment of D-galactose in human plasma, Clin. Chem. 46 (2000) 612–619, https://doi.org/10.1093/clinchem/46.5.612.
[24] M. König, S. Bulik, H.G. Holzhütter, Quantifying the contribution of the liver to glucose homeostasis: a detailed kinetic model of human hepatic glucose metabolism, PLoS Comput. Biol. 8 (2012), https://doi.org/10.1371/journal.pcbi.1002577.
[25] Z.Y. Chen, Z.S. Peng, J. Yang, W.Y. Chen, Z.M. Ou-Yang, A mathematical model for describing light-response curves in Nicotiana tabacum L, Photosynthetica 49 (2011) 467–471, https://doi.org/10.1007/s11099-011-0056-5.
[26] M.P. Hall, J. Unch, B.F. Binkowski, M.P. Valley, B.L. Butler, M.G. Wood, P. Otto, K. Zimmerman, G. Vidugiris, T. MacHleidt, M.B. Robers, H.A. Benink, C.T. Eggers, M.R. Slater, P.L. Meisenheimer, D.H. Klaubert, F. Fan, L.P. Encell, K.V. Wood, Engineered luciferase reporter from a deep sea shrimp utilizing a novel imidazopyrazinone substrate, ACS Chem. Biol. 7 (2012) 1848–1857, https://doi.org/10.1021/cb3002478.
[27] A.M. Loening, T.D. Fenn, A.M. Wu, S.S. Gambhir, Consensus guided mutagenesis of Renilla luciferase yields enhanced stability and light output, Protein Eng. Des. Sel. 19 (2006) 391–400, https://doi.org/10.1093/protein/gzl023.
[28] K. Saito, Y. Chang, K. Horikawa, N. N.H, U, Luminescent proteins for high-speed single-cell and whole-body imaging, Nat. Commun. (2012) 1262, https://doi.org/10.1038/ncomms2248, 2012.
[29] A.M. Smith, Starch in the arabidopsis plant, Starch/Staerke 64 (2012) 421–434, https://doi.org/10.1002/star.201100163.
[30] W.L.O.C.R. Somerville, S.C. Somerville, Isolation of photosynthetically active protoplasts and chloroplasts from Arabidopsis thaliana, Plant Sci. Lett. 21 (1981) 89–96, https://doi.org/10.1007/978-1-60327-210-0_16.
[31] M. Nishimura, T. Akazawa, Photosynthetic activities of spinach leaf protoplasts, Plant Physiol. 55 (1975) 712–716, https://doi.org/10.1104/pp.55.4.712.
[32] I. Farhana, M.N. Hossain, K. Suzuki, T. Matsuda, T. Nagai, Genetically encoded fluorescence/bioluminescence bimodal indicators for Ca2+ imaging, ACS Sens. 4 (2019) 1825–1834, https://doi.org/10.1021/acssensors.9b00531.
[33] P.P. Laissue, R.A. Alghamdi, P. Tomancak, E.G. Reynaud, H. Shroff, Assessing phototoxicity in live fluorescence imaging, Nat. Methods 14 (2017) 657–661, https://doi.org/10.1038/nmeth.4344.
[34] J. Icha, M. Weber, J.C. Waters, C. Norden, Phototoxicity in live fluorescence microscopy, and how to avoid it, Bioessays 39 (2017) 1–15, https://doi.org/10.1002/bies.201700003.
[35] A. Pietraszewska-Bogiel, T.W.J. Gadella, FRET microscopy: from principle to routine technology in cell biology, J. Microsc. 241 (2011) 111–118, https://doi.org/10.1111/j.1365-2818.2010.03437.x.
[36] A. Wang, Q. Jin, X. Xu, A. Miao, J.C. White, J.L. Gardea-Torresdey, R. Ji, L. Zhao, High-throughput screening for engineered nanoparticles that enhance photosynthesis using mesophyll protoplasts, J. Agric. Food Chem. 68 (2020) 3382–3389, https://doi.org/10.1021/acs.jafc.9b06429.
[37] N. Wu, B. Zheng, A. Shaywitz, Y. Dagon, C. Tower, G. Bellinger, C.H. Shen, J. Wen, J. Asara, T.E. McGraw, B.B. Kahn, L.C. Cantley, AMPK-dependent degradation of TXNIP upon energy stress leads to enhanced glucose uptake via GLUT1, Mol. Cell. 49 (2013) 1167–1175, https://doi.org/10.1016/j.molcel.2013.01.035.
[38] S. Rungaldier, W. Oberwagner, U. Salzer, E. Csaszar, R. Prohaska, Stomatin interacts with GLUT1/SLC2A1, band 3/SLC4A1, and aquaporin-1 in human erythrocyte membrane domains, Biochim. Biophys. Acta Biomembr. 1828 (2013) 956–966, https://doi.org/10.1016/j.bbamem.2012.11.030.
[39] S. Iwano, M. Sugiyama, H. Hama, A. Watakabe, N. Hasegawa, T. Kuchimaru, K. Z. Tanaka, M. Takahashi, Y. Ishida, J. Hata, S. Shimozono, K. Namiki, T. Fukano, M. Kiyama, H. Okano, S. Kizaka-kondoh, T.J. Mchugh, T. Yamamori, H. Hioki, S. Maki, A. Miyawaki, Single-cell bioluminescence imaging of deep tissue in freely moving animals, Science 359 (2018) 935–939, https://doi.org/10.1126/science.aaq1067.
[40] S. Inagaki, M. Agetsuma, S. Ohara, T. Iijima, H. Yokota, T. Wazawa, Y. Arai, T. Nagai, Imaging local brain activity of multiple freely moving mice sharing the same environment, Sci. Rep. 9 (2019) 7460, https://doi.org/10.1038/s41598-019-43897-x.